Biomaterials 34 (2013) 1402–1412

Contents lists available at SciVerse ScienceDirect

Biomaterials

journal homepage: www.elsevier.com/locate/biomaterials

Characterization and antibacterial activity of amoxicillin-loaded electrospun nano-hydroxyapatite/poly(lactic-co-glycolic acid) composite nanofibers

Fuyin Zheng [a], Shige Wang [b], Shihui Wen [a], Mingwu Shen [a,**], Meifang Zhu [b], Xiangyang Shi [a,b,c,*]

[a] College of Chemistry, Chemical Engineering and Biotechnology, Donghua University, Shanghai 201620, People's Republic of China
[b] State Key Laboratory for Modification of Chemical Fibers and Polymer Materials, Donghua University, Shanghai 201620, People's Republic of China
[c] CQM – Centro de Química da Madeira, Universidade da Madeira, Campus da Penteada, 9000-390 Funchal, Portugal

ARTICLE INFO

Article history:
Received 19 October 2012
Accepted 30 October 2012
Available online 17 November 2012

Keywords:
Electrospinning
Poly(lactic-co-glycolic acid)
Nano-hydroxyapatite
Amoxicillin
Sustained release
Antibacterial activity

ABSTRACT

We report a facile approach to fabricating electrospun drug-loaded organic/inorganic hybrid nanofibrous system for antibacterial applications. In this study, nano-hydroxyapatite (n-HA) particles loaded with a model drug, amoxicillin (AMX) were dispersed into poly(lactic-co-glycolic acid) (PLGA) solution to form electrospun hybrid nanofibers. The loading of AMX onto n-HA surfaces (AMX/n-HA) and the formation of AMX/n-HA/PLGA composite nanofibers were characterized using different techniques. We show that AMX can be successfully adsorbed onto the n-HA surface and the formed AMX/n-HA/PLGA composite nanofibers have a uniform and smooth morphology with improved mechanical durability. Cell viability assay and cell morphology observation reveal that the formed AMX/n-HA/PLGA composite nanofibers are cytocompatible. Importantly, the loaded AMX within the n-HA/PLGA hybrid nanofibers shows a sustained release profile and a non-compromised activity to inhibit the growth of a model bacterium, *Staphylococcus aureus*. With the significantly reduced burst-release profile, good cytocompatibility, improved mechanical durability, as well as the remained antibacterial activity, the developed AMX/n-HA/PLGA composite nanofibers should find various potential applications in the fields of tissue engineering and pharmaceutical science.

1. Introduction

Electrospinning, a technique producing ultrafine fibers with diameters ranging from tens of nanometers to several microns, has attracted much attention due to its versatility and potential for applications in diverse fields [1–4]. The features of electrospun nanofibers with high specific surface area, high porosity, and three-dimensional (3D) reticulate structure quite mimic the natural extracellular matrix (ECM) [5], affording them with a wide range of biomedical applications including tissue engineering [6], wound dressing [7], biosensors [8], and drug delivery [5,9–12]. In particular for drug delivery applications, conventional [9,13], emulsion [14,15] and coaxial [12] electrospinning techniques have been used to fabricate nanofibers for drug encapsulation and release.

Conventional single fluid electrospinning method allows direct integration of drug molecules within nanofibers by simply electrospinning the drug/polymer mixture solution or post-adsorption of drugs onto/within the nanofibers [11,13,16,17]. However, a burst release often happens, which is not desirable in most of the cases. The techniques of emulsion and coaxial electrospinning used for drug delivery applications are able to alleviate the burst release of the encapsulated drug to some extent [15,18,19]. In both methods, the drugs are able to be incorporated into the core region of the nanofibers to form a "core–sheath" structure, in which the outer polymer shell can act as an additional barrier to control the drug release profile [20]. However, there are still some issues and challenges in the emulsion and coaxial electrospinning techniques. The coaxial electrospinning may need substantial optimization of the electrospinning parameters, and the emulsifier used in emulsion electrospinning may be cytotoxic. In another aspect, the electrospun nanofibers composed of polymer or polymer blends often suffer a problem with mechanical durability, which is not desirable for practical biomedical applications. Therefore, development of other nanofiber systems that possess mitigated burst release of the encapsulated drug and/or improved mechanical durability still remains a great challenge.

* Corresponding author. College of Chemistry, Chemical Engineering and Biotechnology, Donghua University, Shanghai 201620, People's Republic of China. Tel.: +86 21 67792656; fax: +86 21 67792306 804.
** Corresponding author. Tel.: +86 21 67792750; fax: +86 21 67792306 804.
E-mail addresses: mwshen@dhu.edu.cn (M. Shen), xshi@dhu.edu.cn (X. Shi).

0142-9612/$ – see front matter © 2012 Elsevier Ltd. All rights reserved.
http://dx.doi.org/10.1016/j.biomaterials.2012.10.071

In our previous work, we have shown that drug-loaded halloysite nanotubes (HNTs), a naturally occurring clay material, can be incorporated within poly(lactic-co-glycolic acid) (PLGA) nanofibers by simply electrospinning the mixture solution of PLGA and HNTs-drug particles [5]. The thus formed hybrid nanofibers afford the drug with significantly decreased burst release profile, and simultaneously the incorporation of HNTs greatly improves the mechanical durability of the nanofibers [5,21–23]. The incorporated HNTs within the nanofibers play two roles: firstly, the HNTs themselves are a kind of drug carrier, which allows drug molecules to be encapsulated within the lumen of the HNTs; secondly, the presence of HNTs is able to significantly improve the mechanical durability of the nanofibers. The previous success leads us to hypothesize that other inorganic nanoparticles having a capability to encapsulate drug molecules may also be incorporated within polymer nanofibers to alleviate the burst release of drug molecules and to improve the mechanical durability of the fibers, thereby providing a vast range of opportunities for various biomedical applications.

Nano-hydroxyapatite (n-HA) has been considered as an ideal inorganic drug carrier due to its high surface area to volume ratio, high surface activity, good biocompatibility, and strong ability to absorb a variety of chemical species [24]. However, the weak interaction between the drug molecules and the n-HA particles often leads to an initial burst release of the drugs from the formed n-HA/drug nanocomplex [25]. Therefore, it is quite reasonable to design a hybrid n-HA-incorporated polymer nanofiber system, where both polymer nanofibers and the n-HA are containers and barriers of drug molecules, affording the drug with a sustained release profile. Likewise, the presence of n-HA within the polymer nanofibers is also expected to share a portion of load applied on the nanofibrous mats, improving the mechanical durability of the fiber system.

In this present work, we attempted to develop a facile approach to fabricating n-HA-doped PLGA nanofibers via electrospinning for drug encapsulation and release. A model drug, amoxicillin (AMX) was first loaded onto the n-HA surface via physical adsorption. Then the AMX-loaded n-HA particles were mixed with PLGA solution for subsequent formation of electrospun AMX/n-HA/PLGA composite nanofibers (Scheme 1a). The loading of AMX onto n-HA (n-HA/AMX) and the formation of AMX/n-HA/PLGA composite nanofibers were characterized using different techniques. The release kinetics of AMX from the composite AMX/n-HA/PLGA nanofibers was investigated using UV–Vis spectroscopy and compared with AMX/n-HA particles and AMX/PLGA nanofibers. The antimicrobial activity of the AMX/n-HA/PLGA nanofibers was investigated using *Staphylococcus aureus* (*S. aureus*) as a model bacterium both in liquid and on solid medium. The cytocompatibility of AMX/n-HA/PLGA nanofibers was investigated through in vitro 3-(4,5-dimethylthiazol-2-yl)-2,5-diphenyltetrazolium bromide (MTT) viability assay and microscopic imaging of cells cultured onto the composite fibrous scaffolds.

2. Experimental section

2.1. Materials

PLGA (MW = 81 000 g/mol) with a lactic acid/glycolic acid ratio of 50:50 and AMX (purity > 95%) were purchased from Jinan Daigang Biotechnology Co., Ltd. (China) and Shanghai Yuanye Biotechnology Co., Ltd. (China), respectively. n-HA was obtained from Aladdin Chemical Reagent Co., Ltd. (China). *S. aureus* was purchased from Shanghai Fuzhong Biotechnology Development Co., Ltd. (China). Luria-Bertani (LB)-medium was acquired from Sangon Biotech Co., Ltd. (Shanghai, China). Tetrahydrofuran (THF) and N,N-dimethylformamide (DMF) were from Sinopharm Chemical Reagent Co., Ltd. (China). Mouse fibroblasts (L929) were obtained from Institute of Biochemistry and Cell Biology (the Chinese Academy of Sciences, Shanghai, China). Dulbecco's Modified Eagle's Medium (DMEM), fetal bovine serum (FBS), penicillin, and streptomycin were purchased from Hangzhou Jinuo Biomedical Technology (Hangzhou, China). Fluorescein diacetate (FDA) was purchased from Sigma. All chemicals were used as received. Water used in all experiments was purified using a Milli-Q Plus 185 water purification system (Millipore, Bedford, MA) with resistivity higher than 18 MΩ cm.

2.2. Loading of AMX onto the surface of n-HA

An aqueous solution of AMX (10 mL, 4 mg/mL) was added dropwise into an aqueous suspension of sieved n-HA (10 mL, 2 mg/mL). The mixture was then vigorously stirred for 24 h at room temperature to form AMX-loaded n-HA (AMX/n-HA). The formed AMX/n-HA nanohybrid was separated by centrifugation (5000 rpm, 3 min) and washed with water three times to remove the excess free AMX non-adsorbed onto the n-HA surface. The AMX concentration in the supernatant was analyzed using Lambda 25 UV–Vis spectrophotometer (Perkin Elmer, USA) at 228 nm using a standard AMX concentration-absorbance calibration curve and the AMX loading percentage was calculated by Eq. (1):

$$\text{Loading percentage} = M_t/(M_t + M_o) \times 100\% \quad (1)$$

where M_t and M_o stands for the mass of adsorbed AMX and the n-HA carrier, respectively. Finally, the AMX/n-HA was lyophilized, ground down, and sieved to have a uniform size for subsequent electrospinning process. The drug loading

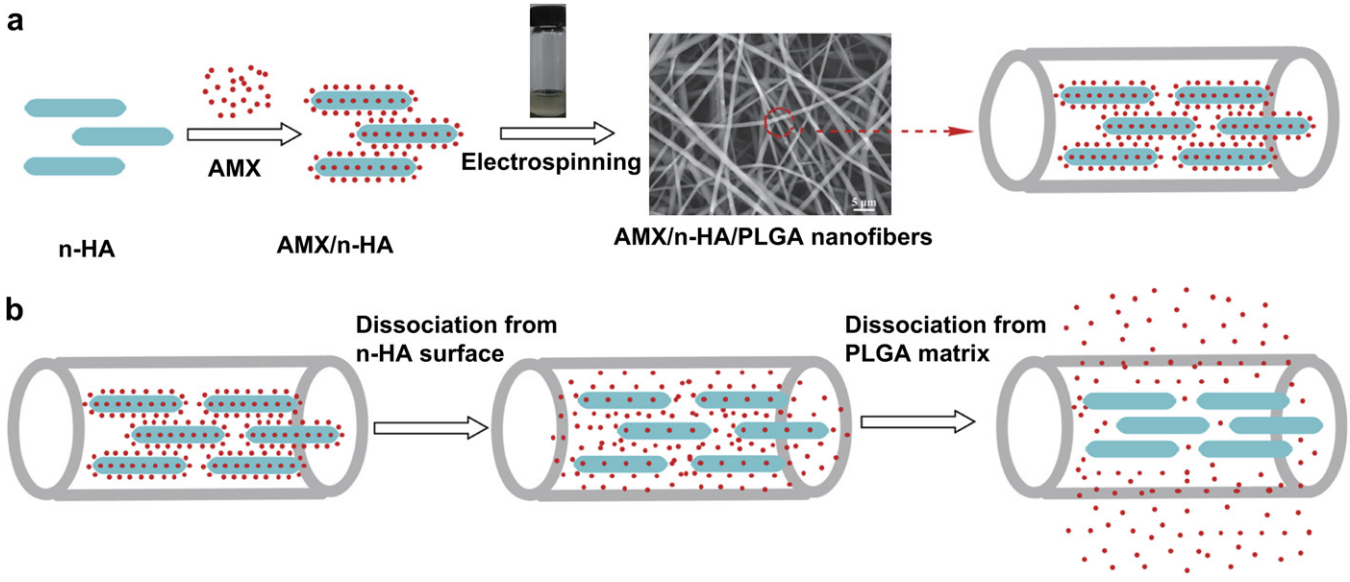

Scheme 1. Schematic illustration of the encapsulation (a) and release pathways (b) of AMX within n-HA-doped PLGA nanofibers.

percentage was optimized by changing the concentrations of AMX and n-HA, respectively.

2.3. Preparation of electrospun AMX/n-HA/PLGA nanofibers

PLGA was dissolved in THF/DMF ($v/v = 3:1$) at an optimized concentration of 25% (w/v, PLGA/solvent) [21,23]. AMX/n-HA powder (1 wt% AMX relative to PLGA) was then blended with PLGA solution for subsequent electrospinning. For comparison, a predetermined amount of n-HA (5 wt% relative to PLGA) or AMX (1 wt% relative to PLGA) was added to PLGA solution and stirred for 1 h to get a homogeneous solution. The electrospun nanofibers were prepared according to the protocol reported in our previous studies [21,23] with a commercial electrospinning equipment (1006 Electrospinning Equipment, Beijing Kang Sente Technology Co., Ltd., Beijing, China) using a stainless steel needle with an inner diameter of 0.8 mm. The electrospinning parameters were set at an applied voltage of 20 kV, a collection distance of 15 cm, and the electrospinning solution flow rate of 1.0 mL/h controlled by a syringe pump.

The percentage of n-HA, AMX/n-HA, and AMX relative to PLGA in the above three cases were 5 wt%, 6 wt%, and 1 wt% (the AMX/n-HA/PLGA nanofibers used in our manuscript was all 1% AMX relative to AMX/n-HA/PLGA nanofibers) if not emphasized, respectively. Note that to prepare AMX/n-HA/PLGA nanofibers, 6 wt% AMX/n-HA (5 wt% n-HA relative to PLGA) was incorporated based on the optimized AMX loading efficiency of 20.45% (see below) to ensure that the concentrations of the incorporated n-HA within both AMX/n-HA/PLGA and n-HA/PLGA nanofibers are approximately similar. The formed electrospun fibrous mats were vacuum dried at ambient temperature for at least 2 d to remove the residual organic solvent and moisture.

2.4. Characterization

The morphology of n-HA before and after AMX loading was observed by transmission electron microscopy (TEM, JZM-2100, Japan) with an operating voltage of 200 kV. Samples were dispersed into water (1 mg/mL) and 5 μL aqueous solution of each sample was dropped onto a carbon-coated copper grid and air-dried before measurement. The incorporation of n-HA within PLGA nanofibers was also confirmed using TEM (Hitachi H-800, Japan) with an operating voltage of 200 kV. Before measurement, the nanofibers were electrospun directly onto holey carbon-coated copper grids. Morphologies of the pure PLGA, n-HA/PLGA, AMX/PLGA, and AMX/n-HA/PLGA nanofibers were observed using scanning electron microscopy (SEM, JEOL JSM-5600LV, Japan). Before SEM observations, the samples were sputter coated with gold films with a thickness of 10 nm. Fiber diameters were measured using Image J 1.40G software (http://rsb.info.nih.gov/ij/down-load.html). At least 100 nanofibers from different SEM images for each sample were randomly selected and analyzed. Fourier transform infrared spectroscopy (FTIR) was performed using a Nicolet Nexus 670 FTIR spectrometer in a wavenumber range of 500–4000 cm^{-1} to confirm the loading of AMX onto the n-HA surface. Dry samples were mixed with milled KBr crystals and the samples were pressed as pellets before measurements. The crystalline structure of n-HA before and after AMX loading was analyzed by a Rigaku D/max-2550 PC XRD system (Rigaku Co., Tokyo, Japan) using Cu Kα radiation with a wavelength of 0.154 nm at 40 kV and 200 mA. The scan was performed from 5° to 70° (2θ).

The porosity of different nanofibers was measured using a method reported in the literature [26]. Five small strips (10×50 mm^2) were cut randomly from the nanofibrous mats. The thickness of the nanofibrous mats was measured with a micrometer and the apparent density (ρ_a) and porosity (p) were calculated from Eqs. (2) and (3), respectively.

$$\rho_a \left(g/cm^3\right) = \frac{m\ (g)}{d\ (cm) \times s\ (cm^2)} \tag{2}$$

$$p = \left(1 - \frac{\rho_a\ (g/cm^3)}{\rho_b\ (g/cm^3)}\right) \times 100\% \tag{3}$$

where m, d, and s stand for mass, thickness, and area of the strips, respectively. The bulk density (ρ_b) of PLGA is 1.25 g/cm^3 [5]. Water contact angle of the electrospun nanofibrous mats was measured using a contact angle goniometer (DSA-30, Kruss, Germany) when the droplet was stable. The electrospun nanofibrous mats were attached to the cover slips and one pendant droplet of distilled water with 1 μL drop size was dropped onto a randomly selected area for each sample at ambient temperature and humidity. Mechanical property evaluation of the nanofibrous mats was performed by a material testing machine (H5K-S, Hounsfield, UK) with a cross-head speed of 10 mm/min under a load of 10 N. The thicknesses of five specimens (10×50 mm^2) were measured with a micrometer and then gripped in the top and bottom chucks, respectively, and the gauge of two chucks connected to testing machine was fixed at 30 mm. The stress and strain data were calculated using Eqs. (4) and (5):

$$\sigma\ (MPa) = \frac{P\ (N)}{w\ (mm) \times d\ (mm)} \tag{4}$$

$$\varepsilon = \frac{l}{l_0} \times 100\% \tag{5}$$

where σ, ε, P, w, d, l, and l_0 stand for stress, strain, load, mat width, mat length, extension length, and gauge length, respectively. Breaking strength, failure strain, and Young's modulus were obtained from the strain–stress curves. All porosity, water contact angle, and mechanical property tests were done in triplicate and the results were reported as mean ± SD.

2.5. In vitro drug release

The release kinetics of AMX from AMX/n-HA particles, AMX/PLGA and AMX/n-HA/PLGA nanofibers was determined by recording the absorbance of AMX at 228 nm using a Lambda 25 UV–Vis spectrophotometer (Perkin Elmer, USA). The AMX/n-HA particles (5 mg) were dispersed into 2 mL phosphate buffer saline (PBS, pH = 7.4) and the solution was transferred into a dialysis tube. Then the dialysis tube was placed in a vial containing 8 mL PBS. For electrospun nanofiber samples, a certain amounts of AMX/PLGA and AMX/n-HA/PLGA nanofibrous mats were weighted and added to different vials containing 10 mL PBS to ensure the amount of AMX contained in both nanofibers is similar to that in the AMX/n-HA sample. All the samples for release experiments were incubated in a vapor-bathing constant temperature vibrator at 37 °C with a vibrating speed of 90 rpm. The experiment was done in triplicate. At the pre-designed time intervals, 1.5 mL of solution of release medium was taken out from each vial and equal volume of fresh PBS was replenished. The accumulated release of AMX was calculated based on a standard AMX absorbance-concentration calibration curve at 228 nm.

2.6. In vitro antibacterial activity assay

S. aureus is a Gram-positive bacterium that can cause a wide range of suppurative infections [27,28]. In this study, *S. aureus* was used as a model bacterium to evaluate the antibacterial activity of AMX adsorbed onto the n-HA surface, or encapsulated within PLGA or n-HA/PLGA composite nanofibers via both quantitative analysis in liquid medium and qualitative analysis on solid medium.

2.6.1. Quantitative analysis in liquid medium

In the quantitative analysis, the frozen *S. aureus* was first activated with fresh LB medium at 37 °C with gentle shaking (100 rpm) in an oscillation incubator. Then, *S. aureus* was added into 5 mL liquid medium with an OD value of 0.1–0.2 at 625 nm for each test tube. After that, AMX, AMX/n-HA particles, and drug-loaded nanofibrous mats (AMX/n-HA/PLGA and AMX/PLGA) with similar AMX concentrations ranging from 0 to 60 μg/mL (relative to the 5-mL bacterial suspension) were added into each test tube. Note that all the samples were sterilized for 3 h before antibacterial testing. The treated bacterial samples were then incubated at 37 °C with gentle shaking (100 rpm), and the absorbance at 625 nm was monitored using Lambda 25 UV–Vis spectrophotometer after 24 h of incubation. Since the absorbance of bacterial solution is in proportion to the number of the bacteria, the percentage of bacterial inhibition can be calculated by the following equation [27]:

$$\text{Bacterial inhibition}\ (\%) = (I_c - I_s)/I_c \times 100 \tag{6}$$

where I_c and I_s are the average ODs of the control group and the experimental group, respectively. To investigate the antibacterial efficacy of the AMX-loaded nanofibers after the release of AMX at a given time period, AMX/PLGA and AMX/n-HA/PLGA nanofibers (with unreleased drug content of 60 μg/mL relative to the 5-mL bacterial suspension) after 4 or 9 days release were also tested under similar conditions.

2.6.2. Qualitative analysis on solid medium

For qualitative analysis, inhibition zone of the *S. aureus* cultured on the LB agar plates was assessed [29]. Briefly, *S. aureus* suspension (100 μL) was first spreaded onto the agar plates and the circular nanofibrous mats (PLGA, n-HA/PLGA, AMX/n-HA/PLGA, and AMX/PLGA) with a diameter of 1 cm and a mass of around 10 mg were pasted onto the agar plate. All the samples were sterilized for 3 h before they were pasted. The amount of AMX in both AMX/n-HA/PLGA and AMX/PLGA nanofibrous mats was approximately 100 μg. The bacteria were then incubated at 37 °C for 24 h and the inhibition zone for each sample on the plate was visually inspected. The inner and outer diameters and calculated diameter difference were measured. To qualitatively evaluate the antibacterial efficacy of the AMX-loaded nanofibers after AMX release, AMX/PLGA and AMX/n-HA/PLGA nanofibers (with unreleased AMX drug of 100 μg) after 4 and 9 days release were also tested under similar conditions.

The antibacterial activity of AMX/n-HA/PLGA nanofibers containing 0.5%, 1%, and 2% AMX relative to PLGA was also tested quantitatively and qualitatively using the above procedures. For the quantitative assay, all of the AMX/n-HA/PLGA nanofibers (20 mg) were added into the test tube containing 5 mL bacterial suspension. For the qualitative assay, all of the AMX/n-HA/PLGA nanofibers were cut into circular mats with a diameter of 1 cm and a mass of around 10 mg.

2.7. Cell culture and cytocompatibility evaluation

Mouse fibroblasts (L929) cells were cultured in a humidified incubator with 5% CO_2 at 37 °C using DMEM containing 10% FBS, 100 U/mL penicillin, and 100 μg/mL streptomycin. MTT assay and SEM observation were employed to evaluate the viability and morphology of the L929 cells cultured onto different nanofibers, respectively. Before cell seeding, PLGA, n-HA/PLGA, and AMX/n-HA/PLGA nanofibrous mats were placed in a 24-well tissue culture plate (TCP) and fixed with stainless steel rings, sterilized with ethanol for 2 h, and soaked with medium overnight. Then, L929 cells were seeded at a density of 1.5×10^4 cells/well for MTT assay and 2×10^4 cells/well for SEM observation, respectively. For comparison, TCPs and cover slips were used as controls.

For MTT assay, after the cells were cultured for 8 or 72 h, the cells were washed with PBS and an MTT solution (40 μL) was added to each well, followed by incubation for another 4 h. Then, 400 μL DMSO was added to each well to dissolve the purple MTT formazan crystal for 15 min and 100 μL of the dissolved formazan solution of each sample was transferred into separate wells of a 96-well plate to test the OD value at 570 nm using a microplate reader (MK3, Thermo, USA). Mean and standard deviation from the triplicate wells for each sample were reported.

To further examine the cytocompatibility of the nanofibers, the morphology of L929 cells grown onto nanofibers, TCPs, or cover slips was observed using SEM. Before analysis, cells grown onto different substrates were washed with PBS, fixed with 2.5% glutaraldehyde for 2 h at 4 °C, dehydrated with a series of gradient ethanol solutions (30, 50, 70, 90, 95, and 100% ethanol, respectively), and air-dried. Then the samples were sputter coated with gold film with a thickness of 10 nm and observed by SEM (JEOL JSM-5600LV, Japan) with an operating voltage of 15 kV.

The attachment and proliferation of L929 cells on nanofiber samples were also observed using Carl Zeiss LSM 700 confocal laser scanning microscope (Jena, Germany). The cells grown on nanofibers and controls with a seeding density of 2×10^4 cells/well after 3 d culture were first fixed with 2.5% glutaraldehyde for 1 h at 4 °C, and then stained by immersing the cells in 1 mL PBS solution containing 0.05 μg/mL FDA for 10 min. The stained L929 cells were observed under excitation wavelength of 494 nm.

2.8. Statistical analysis

One-way ANOVA statistical analysis was performed to compare the bacterial inhibition effect of the tested materials with different AMX concentrations in liquid medium and the cytocompatibility of cells cultured onto different materials. 0.05 was selected as the significance level, and the data were indicated with (*) for $p < 0.05$, (**) for $p < 0.01$, and (***) for $p < 0.001$, respectively.

3. Results and discussion

3.1. Loading of AMX onto the n-HA surfaces

n-HA with a structural formula of $Ca_{10}(PO_4)_6(OH)_2$ is the principal inorganic ingredient of bone and teeth of the mammal [30]. Due to the high surface area and the resultant excellent absorption capability, n-HA has been widely used in various drug delivery applications [25,31,32]. Different from our previous study related to the drug encapsulation within the lumen of HNTs [5], in this study, commercial rod-like n-HA with a diameter of 37 ± 9 nm and a length of 118 ± 42 nm (Fig. 1a) was used to load drug AMX on its surface (Scheme 1a).

The loading percentage of AMX onto n-HA was optimized by varying the respective concentration of AMX and n-HA under similar experimental conditions. Fig. 2 shows the profile of the AMX loading percentage as a function of AMX concentration under different n-HA concentrations. It is clear that the AMX loading percentage increases with the AMX concentration but decreases with the n-HA concentration. This could be attributable to the aggregation of the n-HA at a higher concentration, leading to relatively limited n-HA surface area to be accessed by the AMX molecules. It is worth noting that at n-HA concentration of 1 mg/mL, the used AMX concentration cannot be greater than 2 mg/mL due to the limited solubility of AMX in water (pH 5.5–6.0) [33]. Therefore, 2 mg/mL is considered to be a saturation concentration of AMX when n-HA concentration is 1 mg/mL and the optimized

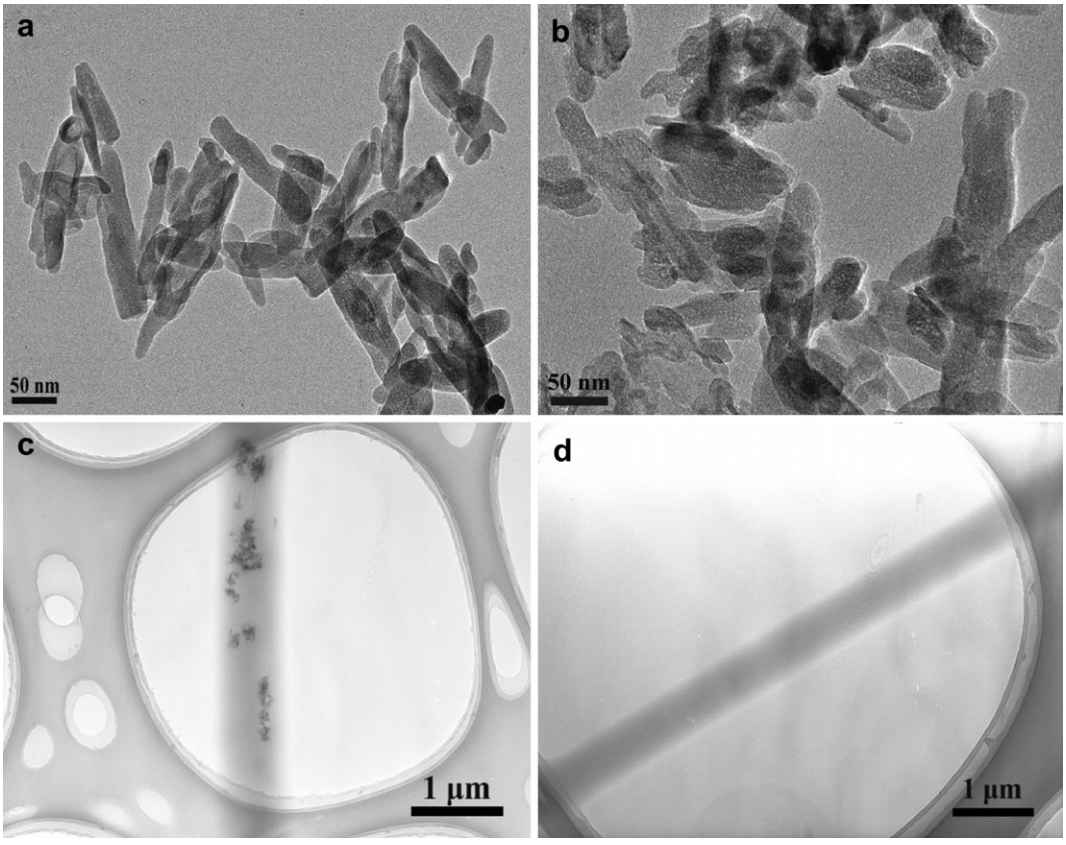

Fig. 1. TEM micrographs of n-HA particles (a), AMX/n-HA particles (b), n-HA/PLGA nanofibers (c), and pure PLGA nanofibers without n-HA loading (d), respectively.

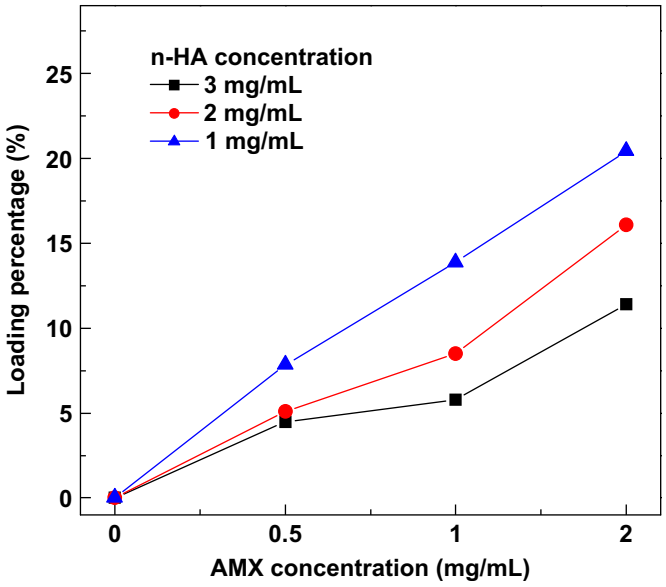

Fig. 2. The AMX loading percentage as a function of AMX concentration under different n-HA concentrations.

AMX loading percentage is 20.45% at the optimized concentration of AMX (2 mg/mL) and n-HA (1 mg/mL).

The successful loading of AMX onto the n-HA surface was qualitatively confirmed by FTIR spectroscopy (Fig. 3). In Fig. 3a, the typical absorption bands at 1686 cm^{-1} and 1519 cm^{-1} can be assigned to the amide I and amide II bond of AMX, respectively. The peaks at 1618 cm^{-1}, 1775 cm^{-1} and 1018 cm^{-1} may be attributed to the absorption band of benzene ring, the vibration of carboxyl group, and the stretching vibration of C–S group of the AMX, respectively. The peak at 3448 cm^{-1} is due to the stretching vibration of amino and hydroxyl group in the AMX structure. [34,35]. In Fig. 3b (Curve 1), a broad peak at 3448 cm^{-1} is assigned to the stretching of OH-group and the band at 1630 cm^{-1} is ascribed to the in-plane bending of OH-group in n-HA. The absorption peaks at 1111 cm^{-1} and 1044 cm^{-1} may be due to the stretching vibrations of phosphate group and peaks at 603 and 567 cm^{-1} are due to bending vibrations of phosphate group [36]. Compared with the spectrum of n-HA (Fig. 3b, Curve 1), new peaks emerged at 1767 and 1617 cm^{-1} in the spectrum of AMX/n-HA (Fig. 3b, Curve 2) and the peak position was shifted from 1630 cm^{-1} to 1638 cm^{-1} after n-HA loading. These peaks are probably due to the combination and overlap of AMX peaks at 1775, 1686 and 1618 cm^{-1} (Fig. 3a) and the n-HA peak at 1630 cm^{-1} (Fig. 3b, Curve 1). Besides, compared to the absorption bands of n-HA, the absorption bands at 3448 and 1044 cm^{-1} (Fig. 3b, Curve 2) could be attributed to the introduction of AMX with peaks at both 3448 cm^{-1} and 1018 cm^{-1}. The FTIR data qualitatively verified the loading of AMX onto the n-HA surfaces. Some other AMX signals was difficult to be observed in the AMX/n-HA sample, likely due to the insensitivity of the FTIR technique or the fact that the vibration bands of AMX are overlapped with those of the n-HA.

XRD was used to characterize the crystalline structure of n-HA before and after the loading of AMX onto n-HA surfaces (Fig. S1a, Supporting information). It can be seen that most of the indexed diffraction peaks of the n-HA (Joint Committee for Powder Diffraction Standards standard X-ray diffraction data for pure hydroxyapatite: 09-0432) are similar to those of n-HA after encapsulation of AMX drug. The intensity of some of the typical n-HA diffraction peaks (e.g., the (002) at 25.8° and the (211) at 31.8°) was decreased after loading of AMX onto n-HA, possibly due to the surface adsorption of the AMX molecules. Further careful analysis of the diffraction angle and plane spacing (Table S1, Supporting information) reveals that the loading of AMX results in the shift of 2θ peak positions of (210) and (202) planes to lower angles (from 29.02 to 28.75° for (210) and from 35.48 to 34° for (202), respectively), and the slight enlargement of the plane spacing (from 3.074 to 3.103 Å for (210) and from 2.528 to 2.635 Å for (202), respectively). This indicates that the AMX adsorption onto n-HA surfaces preferentially occurs on the (210) and (202) planes and the AMX loading does not change the crystalline structure of n-HA. The peaks related to the AMX drug (Figure S1b, Supporting information) do not appear in the XRD pattern of AMX/n-HA, likely due to the fact that the loaded amount of AMX drug is too low to be detectable by XRD technology.

The morphology of n-HA before and after AMX loading was observed via TEM (Fig. 1a and b). It is clear that after drug loading, the n-HA still maintains its original rod-like shape with similar length and width, suggesting that the drug loading process does not appreciably change the morphology of the n-HA. The driving force to load AMX onto the n-HA surfaces is believed to be the hydrogen bonding formation between the AMX hydroxyl, carboxyl, or amine groups and the hydroxyl groups of n-HA, although some other weak forces may also exist.

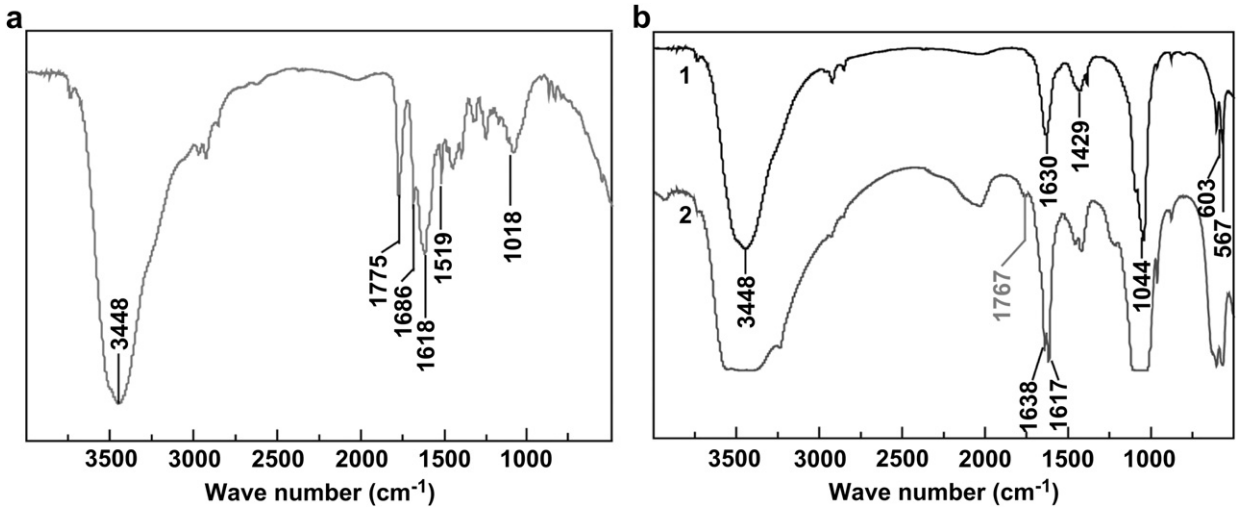

Fig. 3. FTIR spectra of free AMX (a), and n-HA before (Curve 1) and after (Curve 2) AMX loading (b).

3.2. Fabrication of electrospun AMX/n-HA/PLGA nanofibers

The formed AMX/n-HA particles with optimized AMX loading percentage were then doped with PLGA nanofibers via electrospinning to form AMX/n-HA/PLGA composite nanofibers (Scheme 1a). For comparison, pure PLGA nanofibers, n-HA-doped PLGA nanofibers without AMX and AMX-doped PLGA nanofibers without n-HA were also fabricated under similar electrospinning

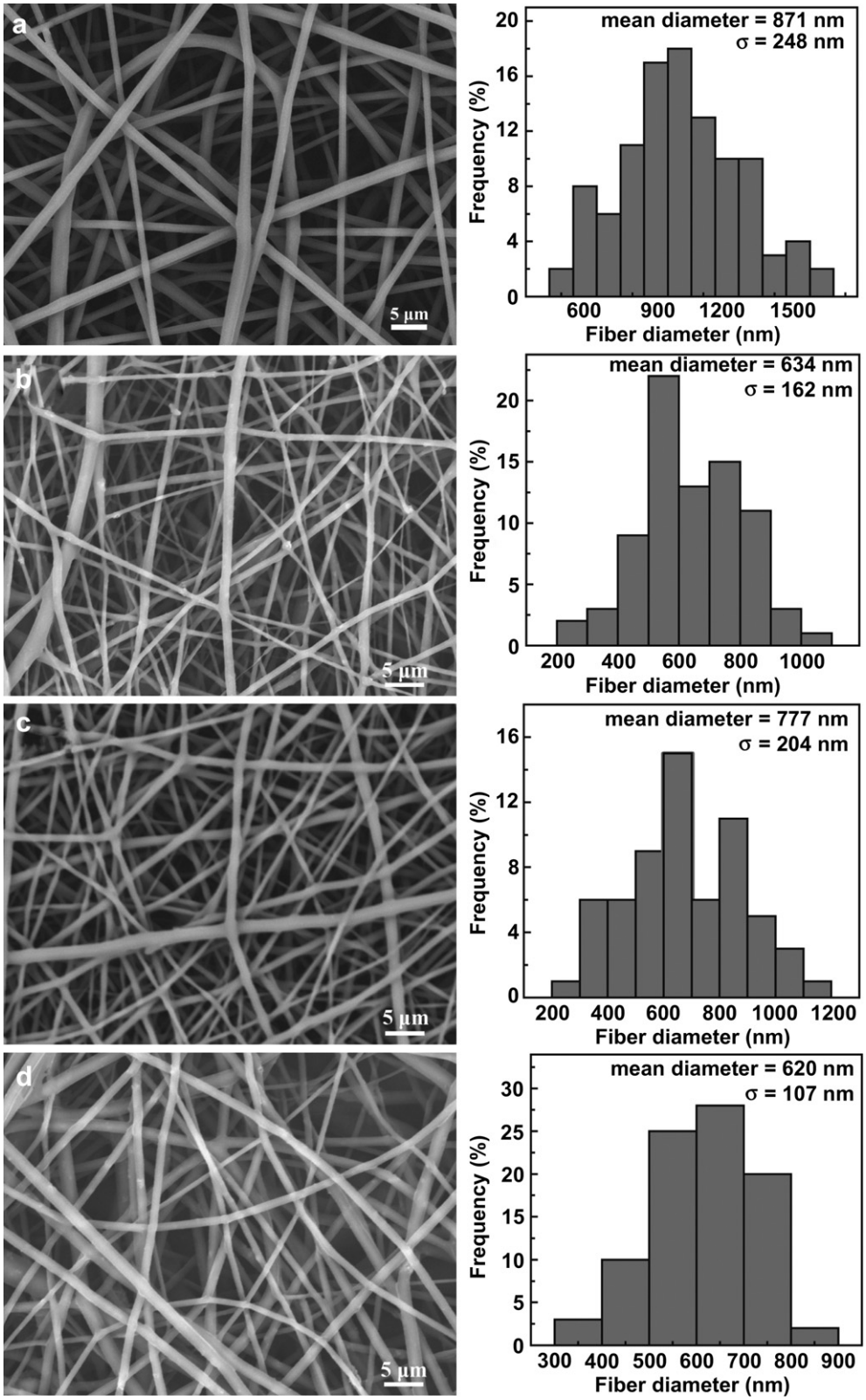

Fig. 4. SEM micrographs and diameter distribution histograms of electrospun PLGA fibers (a), n-HA/PLGA composite fibers (5 wt% n-HA relative to PLGA) (b), AMX/PLGA composite fibers (1 wt% AMX relative to PLGA) (c), and AMX/n-HA/PLGA composite fibers (5 wt% n-HA and 1% AMX both relative to PLGA) (d), respectively.

conditions. The existence of n-HA within n-HA/PLGA composite nanofibers was visually confirmed by TEM (Fig. 1c). In contrast, in the TEM image of pure PLGA nanofiber without n-HA incorporation (Fig. 1d), there are no somewhat aggregated n-HA particles within the fibers.

The surface morphology of the PLGA, n-HA/PLGA, AMX/PLGA, AMX/n-HA/PLGA nanofibers were observed via SEM (Fig. 4). With the easy electrospinnability of PLGA [21,37,38], the incorporation of n-HA, AMX, or AMX-loaded n-HA does not seem to significantly alter the uniform and smooth fibrous morphology of PLGA nanofibers. The diameters of the electrospun PLGA nanofibers (Fig. 4a), n-HA/PLGA (Fig. 4b), AMX/PLGA (Fig. 4c), and AMX/n-HA/PLGA composite nanofibers (Fig. 4d) were estimated to be 871 ± 248 nm, 634 ± 162 nm, 777 ± 202 nm, and 620 ± 107 nm, respectively. The smaller diameters of the n-HA/PLGA, AMX/PLGA, and AMX/n-HA/PLGA composite nanofibers than that of pure PLGA nanofibers are presumably due to the increase of the solution conductivity or the solution viscosity, which was caused by the introduction of n-HA or AMX species in the electrospinning solution.

Porosity, surface hydrophilicity, and mechanical durability are important parameters for the electrospun nanofibers to be used in biomedical applications. The porosity and water contact angle data of PLGA, n-HA/PLGA, AMX/n-HA/PLGA nanofibers are listed in Table 1. It is clear that the addition of a small amount of n-HA (5 wt% relative to PLGA) or AMX/n-HA (6 wt% relative to PLGA) does not significantly change the porosity and the hydrophilicity of the mats. The mechanical property data of electrospun PLGA, n-HA/PLGA, AMX/n-HA/PLGA nanofibers are summarized in Table S2 (Supporting information) and the corresponding representative strain–stress curves are shown in Fig. 5. Compared with PLGA fibrous mats, the failure strain of either n-HA/PLGA or AMX/n-HA/PLGA nanofibers was decreased, while the breaking strength and Young's modulus of both n-HA/PLGA and AMX/n-HA/PLGA were significantly increased. This is likely due to the presence of n-HA in the PLGA fibers, which enables an efficient load transfer from the PLGA matrix to the n-HA rods, in agreement with our previous work related to HNT-doped PLGA nanofibers [5]. The decreased failure strain may be ascribed to the increased brittleness of the nanofibers after incorporation of the n-HA.

3.3. Release of AMX from AMX/n-HA/PLGA composite nanofibers

The release profiles of AMX from AMX/n-HA rods, electrospun AMX/PLGA nanofibers, and AMX/n-HA/PLGA nanofibers are shown in Fig. 6. It is clear that both AMX/n-HA rods and the AMX/PLGA nanofibers (1 wt% AMX relative to PLGA) exhibit an obvious initial burst release. Within the first 24 h, approximate 50% of the drug was released and most of the remaining drug (total release percentage >90%) was released within the successive 6 days at a slightly slower speed. In contrast, the AMX release from the AMX/n-HA/PLGA fibers followed a biphasic pattern characterized by an initial fast release and a successive sustained release phase. About 16% of the AMX was released within the first 24 h, and around 35% AMX was released on the day 18.

Table 1
Apparent density, porosity and water contact angle of PLGA, n-HA/PLGA, and AMX/n-HA/PLGA nanofibers (data are representatives of independent experiments and all data are given as mean ± SD, $n = 5$).

Sample	Apparent density (g/cm^3)	Porosity (%)	Water contact angle (°)
PLGA	0.357 ± 0.087	71.5 ± 6.9	139.2 ± 2.1
n-HA/PLGA	0.357 ± 0.067	71.4 ± 5.4	136.3 ± 2.2
AMX/n-HA/PLGA	0.315 ± 0.02	74.8 ± 1.6	137.2 ± 2.9

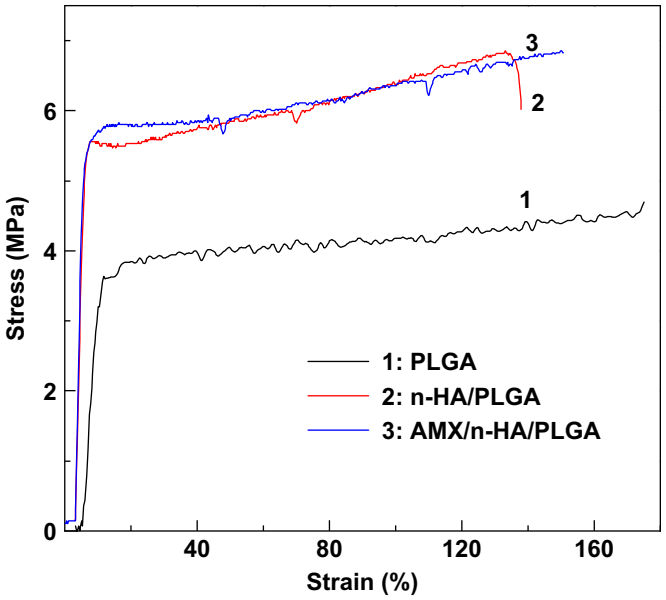

Fig. 5. Representative stress–strain curves of electrospun PLGA (Curve 1), n-HA/PLGA (5 wt% n-HA relative to PLGA, Curve 2), and AMX/n-HA/PLGA (1 wt% AMX relative to PLGA, Curve 3) nanofibrous mats.

The fast release of AMX from AMX/n-HA rods is thought to be due to the fact that the physical interaction between AMX and n-HA (e.g., hydrogen bonding) is not sufficiently strong. The same fast release of AMX from AMX/PLGA nanofibers is easily understandable, because the direct physical integration of drugs within polymer nanofibers gives rise to a matrix-type drug release featured with a fast release rate, in agreement with our previous work [5]. Therefore, for both AMX/n-HA and AMX/PLGA drug carrier systems, the weak force between the drug and the carriers unavoidably leads to an initial burst release of the drug. However, for AMX/n-HA/PLGA drug carrier system, the encapsulated AMX drug should first be dissociated from the n-HA surface to the solid PLGA matrix, and then be released from the solid PLGA matrix to the outer phase

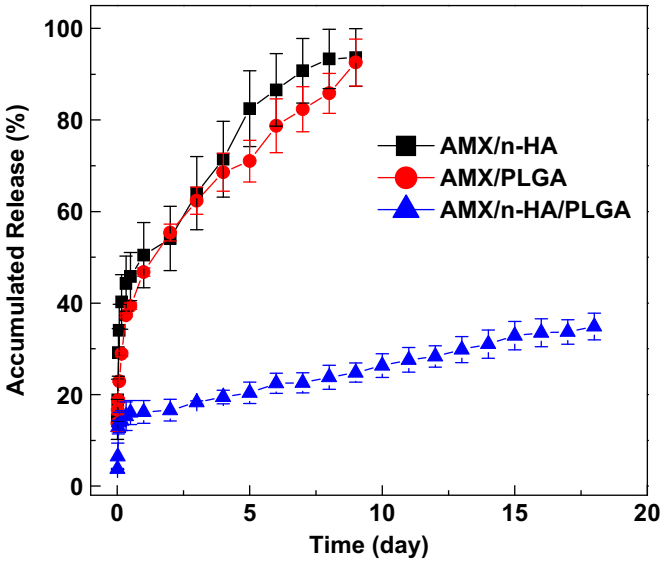

Fig. 6. In vitro release of AMX from AMX/n-HA rods and electrospun AMX/PLGA (1 wt% AMX relative to PLGA) and AMX/n-HA/PLGA (1 wt% AMX relative to PLGA) nanofibers with similar AMX amount. The samples were incubated in PBS buffer (pH = 7.4) at 37 °C.

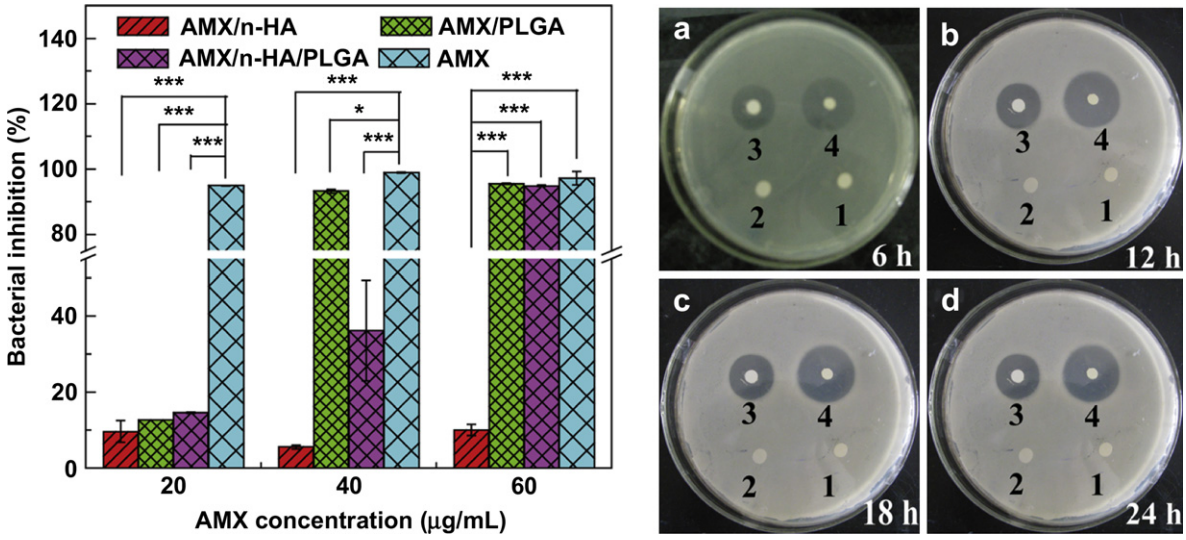

Fig. 7. Left panel: inhibition of bacterial (*S. aureus*) growth as a function of the AMX concentration after 24 h incubation of free AMX, AMX/n-HA particles, AMX/PLGA nanofibers, and AMX/n-HA/PLGA nanofibers, respectively. Right panel: Growth inhibition of bacteria (*S. aureus*) on agar plate at the incubation time of 6 h (a), 12 h (b), 18 h (c), and 24 h (d). Spot 1, 2, 3, and 4 represents PLGA, n-HA/PLGA, AMX/n-HA/PLGA, and AMX/PLGA nanofibers, respectively.

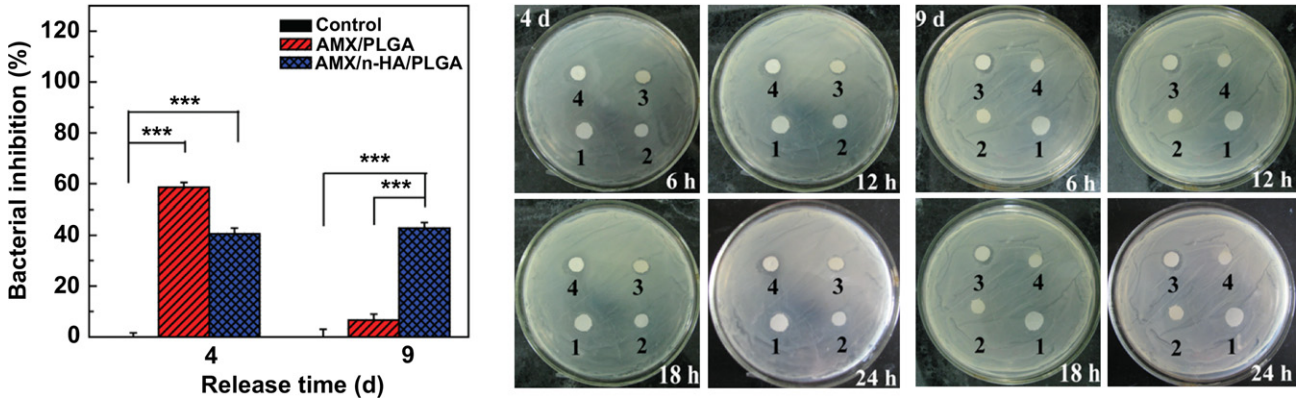

Fig. 8. Left panel: Inhibition of bacterial (*S. aureus*) growth using AMX-loaded nanofibers (original unreleased AMX content was 60 μg/mL relative to the 5-mL bacterial suspension) after 4 or 9 days release after 24 h incubation. Untreated bacterial solution was set as control. Middle and right panels: Growth inhibition of bacteria (*S. aureus*) on agar plate at the incubation time of 6 h, 12 h, 18 h, and 24 h using AMX-loaded nanofibers after 4 (middle panel) or 9 (right panel) days release. Spots 1–4 represents PLGA, n-HA/PLGA, AMX/n-HA/PLGA, and AMX/PLGA nanofibers, respectively.

solution (Scheme 1b). With the combination of two different dissociation pathways, the diffusion rate of the AMX drug is significantly slowed down, thereby achieving a sustained release profile. The first-stage slight burst release of AMX should be attributed to the matrix-type release of AMX pre-dissociated from n-HA surfaces during the electrospinning process. It should be noted that with the inherent property of n-HA particles that are easy to form a certain degree of aggregation (Fig. 1a), it is inevitable to see the same aggregated structure of AMX/n-HA rods within the PLGA nanofibers (Fig. 1c). As long as the percentage of AMX/n-HA particles within the PLGA nanofibers is controlled to be similar and the aggregation behavior of AMX/n-HA particles within the PLGA nanofibers is similar, the release kinetics data should be reproducible.

3.4. Antibacterial activity

We next explored the antibacterial activity of the AMX/n-HA/PLGA composite nanofibers. The antibacterial bioactivity of free AMX, AMX/n-HA rods, and AMX/PLGA nanofibers with different AMX concentrations was also evaluated for comparison (Fig. 7, left panel). The quantitative analyses in liquid medium show that the antibacterial activity of the AMX/HA/PLGA nanofibers is concentration-dependent and lower AMX concentrations (20 or 40 μg/mL) do not induce more than 90% bacterial inhibition. This is presumably due to the slow release rate of AMX at 24 h within n-HA/PLGA composite nanofibers, and the initial fast released AMX is not sufficiently concentrated for effective bacterial inhibition. Therefore, only at the AMX concentration of 60 μg/mL, the AMX/n-HA/PLGA nanofibers have more than 90% bacterial inhibition efficacy and there is no significant difference in comparison with free

Table 2
Diameters of bacterial inhibition rings for different samples at different release time periods.

Release time	Samples	External diameter (cm)	Inner diameter (cm)	Diameter difference (cm)
4 d	AMX/n-HA/PLGA	1.41 ± 0.044	1.00 ± 0.072	0.41 ± 0.05
	AMX/PLGA	1.59 ± 0.19	1.09 ± 0.01	0.50 ± 0.20
9 d	AMX/n-HA/PLGA	1.44 ± 0.15	1.07 ± 0.15	0.37 ± 0.015
	AMX/PLGA	–	–	–

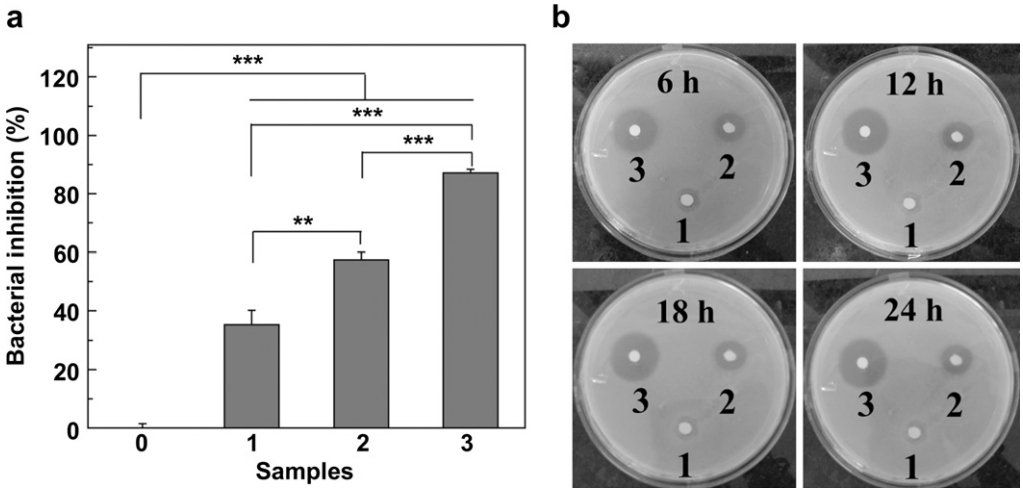

Fig. 9. (a) Inhibition of bacterial (*S. aureus*) growth in liquid medium after 24 h incubation of AMX/n-HA/PLGA nanofibers. Sample 0, 1, 2 and 3 represents control bacterial solution without treatment (0), and bacterial solution treated with 0.5% AMX/n-HA/PLGA (1), 1% AMX/n-HA/PLGA (2), and 2% AMX/n-HA/PLGA (3) nanofibers, respectively. (b) Growth inhibition of bacteria (*S. aureus*) on agar plate at the incubation time of 6 h, 12 h, 18 h, and 24 h. spot 1, 2, and 3 represents 0.5% AMX/n-HA/PLGA, 1% AMX/n-HA/PLGA, and 2% AMX/n-HA/PLGA nanofibers, respectively.

AMX and AMX/PLGA nanofibers ($p > 0.05$). In contrast, free AMX is able to effectively inhibit the bacterial growth with more than 95% efficiency at all the studied AMX concentrations. The bacterial inhibition percentage of 93.2% for AMX/PLGA nanofibers at the AMX concentration of 40 μg/mL is believed to be due to the relatively fast release of AMX from the AMX/PLGA nanofibers. At AMX concentration of 20 μg/mL, the bacterial inhibition percentages of AMX/n-HA, AMX/PLGA, and AMX/n-HA/PLGA are quite similar and are around 10%, which is due to the lower amount of AMX released at such a low AMX concentration. Interestingly, the AMX/n-HA rods display a very low bacterial inhibition percentage of <10% at all studied AMX concentrations. We think that it is probably due to the strong adsorption of medium protein on the surface of AMX/n-HA rods, significantly restraining the release of AMX. Further, control samples of PLGA and n-HA/PLGA nanofibers without AMX loading do not display any bacterial inhibition effect (data not shown).

The bacterial inhibition efficacy of the AMX-loaded nanofibers was further examined by qualitative analysis using a disk diffusion method (Fig. 7, right panel). It is clear that PLGA and n-HA/PLGA nanofibers without AMX encapsulation do not display bacterial inhibition rings at all the studied time points. In contrast, an obvious bacterial inhibition ring on the AMX/PLGA nanofibers (Fig. 7 right, a–d, spot 4) can be seen at all the time points. The bacterial inhibition ring on the AMX/n-HA/PLGA nanofibers is smaller than that on the AMX/PLGA nanofibers at different time points (Fig. 7 right, a–d, spot 3), which is due to the lower concentration of AMX released from the AMX/n-HA/PLGA nanofibers with a quite low release rate. Taken together with the quantitative analysis data, our results clearly suggest that the loading of AMX within n-HA/PLGA nanofibers does not compromise its antibacterial activity, and the sustained release profile with slow release rate may be beneficial for maintaining the long-term antibacterial effect of the AMX drug.

Table 3
Diameters of bacterial inhibition rings for AMX/n-HA/PLGA nanofibers with different encapsulated drug contents.

Samples	External diameter (cm)	Inner diameter (cm)	Diameter difference (cm)
0.5% AMX/n-HA/PLGA	1.25 ± 0.015	0.64 ± 0.015	0.60 ± 0.02
1% AMX/n-HA/PLGA	1.99 ± 0.02	0.65 ± 0.010	1.34 ± 0.01
2% AMX/n-HA/PLGA	2.67 ± 0.02	0.64 ± 0.02	2.03 ± 0.005

The antibacterial activity of AMX/PLGA and AMX/n-HA/PLGA nanofibers after 4 or 9 days release was also studied both quantitatively and qualitatively. As shown in Fig. 8 (left panel), the antibacterial efficiency of AMX/PLGA and AMX/n-HA/PLGA nanofibers is 58.6% and 40.5%, respectively after 4 days release ($p < 0.001$ compared with control group). However, after 9 days release, the antibacterial activity of AMX/PLGA nanofibers was much less effective than that after 4 days release, which is likely due to the fact that a significant portion of AMX was released on day 9 (Fig. 6). In contrast, the AMX/n-HA/PLGA nanofibers were still able to efficiently inhibit the bacterial growth with a bacterial inhibition efficiency of 42.8% (significantly higher than the control and the AMX/PLGA groups, $p < 0.001$). The qualitative antibacterial results

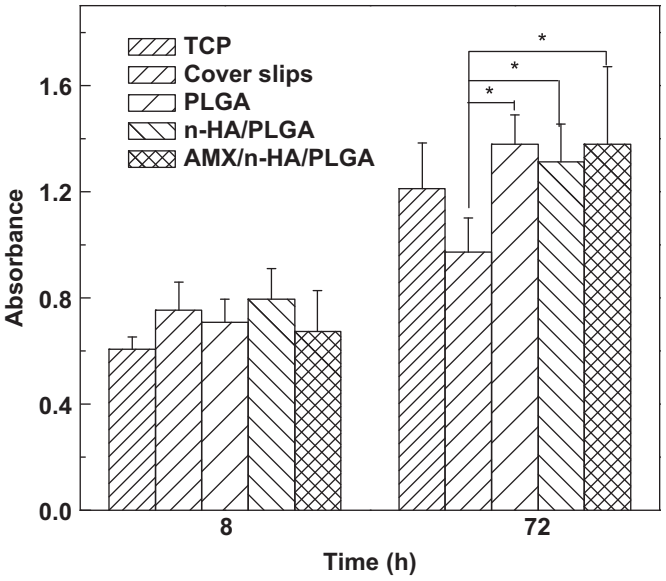

Fig. 10. MTT assay of the attachment and proliferation viability of L929 cells cultured onto TCPs, cover slips, PLGA nanofibers, n-HA/PLGA nanofibers, and AMX/n-HA/PLGA nanofibers, respectively.

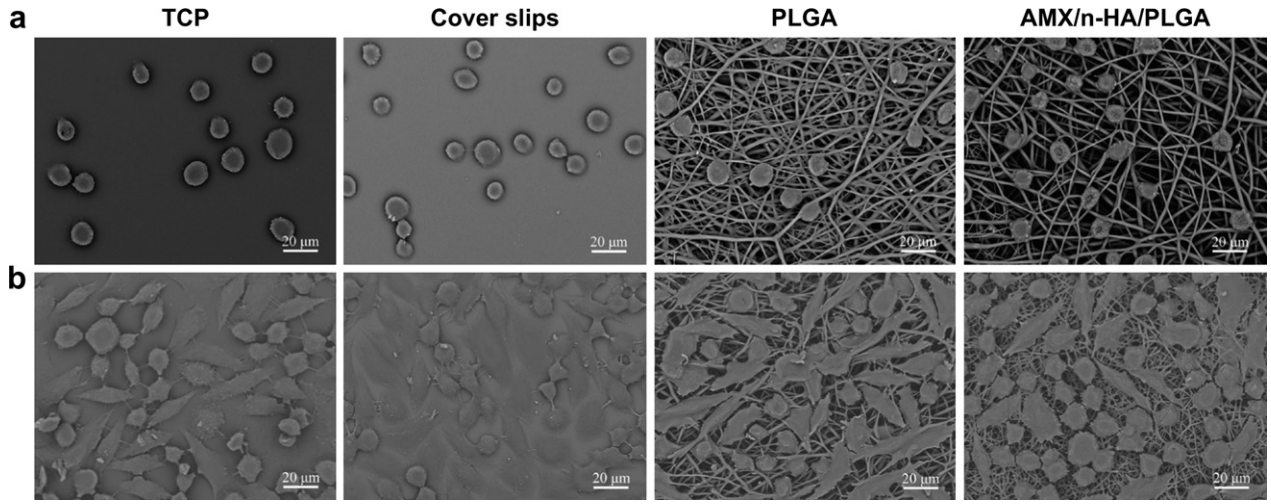

Fig. 11. SEM micrographs of L929 cells grown onto TCPs, cover slips, PLGA nnaofibers, and AMX/n-HA/PLGA nanofibers after 8-h (a) and 3-day (b) culture, respectively.

can be also seen in Fig. 8 (middle and right panels). It is clear that PLGA and n-HA/PLGA nanofibers without AMX loading do not have antibacterial effect at all time points. In contrast, both AMX/PLGA and AMX/n-HA/PLGA nanofibers show visible bacterial inhibition rings after 4 days release. The specific diameters of bacterial inhibition rings are listed in Table 2. It can be seen that after 4 days release, the diameter difference for AMX/PLGA nanofibers is larger than that for AMX/n-HA/PLGA nanofibers. In sharp contrast, after 9 days release, no obvious bacterial inhibition rings can be found for AMX/PLGA nanofibers, while AMX/n-HA/PLGA nanofibers still reserve significant bacterial inhibit activity. Both the quantitative and qualitative antibacterial assay results clearly suggest that AMX/n-HA/PLGA nanofibers have long-term antibacterial activity, which is very important for biomedical applications requiring long-term therapeutic activity.

We further investigated the influence of the encapsulated amount of AMX/n-HA particles on the antibacterial activity of the AMX/n-HA/PLGA nanofibers (Fig. 9). Obviously, all of the AMX/n-HA/PLGA nanofibers (0.5%, 1%, and 2% AMX relative to PLGA, respectively) are able to significantly inhibit the bacterial growth ($p < 0.001$ for all cases compared with the control group), and the bacterial inhibition percentage significantly increases with the doped AMX amount (Fig. 9a). Qualitatively, the diameter of the bacterial inhibition rings also increases with the encapsulated AMX amount at each time point (Fig. 9b and Table 3). These data clearly indicate that AMX/n-HA/PLGA nanofibers show a concentration-dependent antibacterial activity both in liquid and on solid medium.

3.5. Cytocompatibility assay

For further biomedical applications, it is important to ensure the biocompatibility of the developed nanofibrous materials. The cytocompatibility of AMX/n-HA/PLGA nanofibers was assessed by MTT viability assay of L929 cells cultured onto the fibrous materials in comparison with the control materials of TCPs, cover slips, PLGA, and n-HA/PLGA nanofibers (Fig. 10). It is clear that the attachment viability of L929 cells cultured onto TCPs, cover slips, and all fiber samples do not show statistical significant difference after 8 h culture ($p > 0.05$). At the time point of 72 h, the viability of cells cultured onto all materials is much higher than that cultured onto the corresponding material at 8 h ($p < 0.05$). And the viability of cells cultured onto all fibrous materials (PLGA, n-HA/PLGA, and AMX/n-HA/PLGA nanofibers) is much higher than that onto cover slips ($p < 0.05$) and shows no difference from that onto TCPs ($p > 0.05$), suggesting that the incorporation of n-HA or AMX/n-HA does not compromise the cytocompatibility of PLGA nanofibers.

The cytocompatibility of the AMX/n-HA/PLGA nanofibers was further confirmed by observing the morphology of cells cultured onto the nanofibrous scaffold after 3 d via confocal microscopy (Fig. S2, Supporting information). The viable cells can be visually observed after FDA staining with green fluorescence. It is clear that L929 cells cultured onto the PLGA and AMX/n-HA/PLGA fibrous mats show a phenotypic shape with better cell migration. The loading of AMX drug within n-HA/PLGA nanofibers does not seem to change the cell morphology in comparison with that cultured onto n-HA/PLGA nanofibers without AMX (Fig. S3, Supporting information). In contrast, cells grown onto both cover clips and TCPs display a regular spindle shape. The morphology of cells cultured onto different substrates was also observed by SEM (Fig. 11). It can be seen that PLGA and AMX/n-HA/PLGA fibrous mats have similar cell attachment viability to the controls of TCPs and cover slips after 8 h culture, and the nanofibrous mats are able to allow the cells to display a phenotypic shape after 3 d culture, indicating that the cells can penetrate and migrate within the scaffolds in a manner similar to native ECM. Similar to the confocal microscopic imaging data, SEM shows that cells cultured onto the AMX-loaded n-HA/PLGA nanofibers have similar morphology to those cultured onto n-HA/PLGA nanofibers without drug loading (Fig. S4, Supporting information). These cell morphology observation data corroborate the results of MTT assay.

4. Conclusion

In summary, we developed a facile approach to fabricating smooth and uniform AMX/n-HA/PLGA composite nanofibers with improved AMX release profile, and non-compromised antibacterial activity of the AMX drug. The incorporation of drug-loaded n-HA not only significantly improved the mechanical durability of the nanofibers, but also appreciably weakened the initial burst release of the drug. The combination of two pathways for the AMX dissociation first from n-HA surface to PLGA fiber matrix and then from PLGA fiber matrix to the release medium is proven to be an efficient strategy to slow down the release rate of AMX, which is important for biomedical applications requiring the drug to maintain long-term antibacterial efficacy. With the proven cytocompatibility of the composite nanofibers, the concept to design n-HA/PLGA nanofiber-based drug carrier may be extended to prepare other

drug delivery systems for various applications in tissue engineering and pharmaceutical science.

Acknowledgements

Shige Wang and Fuyin Zheng equally contributed to this work. This research is financially supported by the High-Tech Research and Development Program of China (2012AA030309), "111 Project", B07024, the Program for New Century Excellent Talents in University, State Education Ministry, the Fund of the Science and Technology Commission of Shanghai Municipality (11nm0506400), and the Fundamental Research Funds for the Central Universities (for M.S. and X.S.). M.Z. thanks the National Natural Science Foundation of China (50925312) for support. X.S. gratefully acknowledges the Fundação para a Ciência e a Tecnologia (FCT) and Santander bank for the Invited Chair in Nanotechnology.

Appendix A. Supplementary data

Supplementary data related to this article can be found at http://dx.doi.org/10.1016/j.biomaterials.2012.10.071.

References

[1] Doshi J, Reneker DH. Electrospinning process and applications of electrospun fibers. J Electrost 1995;35:151–60.
[2] Dzenis Y. Spinning continuous fibers for nanotechnology. Science 2004;304:1917–9.
[3] Huang ZM, Zhang YZ, Kotaki M, Ramakrishna S. A review on polymer nanofibers by electrospinning and their applications in nanocomposites. Compos Sci Technol 2003;63:2223–53.
[4] Reneker DH, Chun I. Nanometre diameter fibres of polymer, produced by electrospinning. Nanotechnology 1996;7:216.
[5] Qi R, Guo R, Shen M, Cao X, Zhang L, Xu J, et al. Electrospun poly (lactic-co-glycolic acid)/halloysite nanotube composite nanofibers for drug encapsulation and sustained release. J Mater Chem 2010;20:10622–9.
[6] Li WJ, Laurencin CT, Caterson EJ, Tuan RS, Ko FK. Electrospun nanofibrous structure: a novel scaffold for tissue engineering. J Biomed Mater Res 2002;60:613–21.
[7] Khil MS, Cha DI, Kim HY, Kim IS, Bhattarai N. Electrospun nanofibrous polyurethane membrane as wound dressing. J Biomed Mater Res Part B 2003;67:675–9.
[8] Ding B, Wang M, Wang X, Yu J, Sun G. Electrospun nanomaterials for ultrasensitive sensors. Mater Today 2010;13:16–27.
[9] Zeng J, Xu X, Chen X, Liang Q, Bian X, Yang L, et al. Biodegradable electrospun fibers for drug delivery. J Control Release 2003;92:227–31.
[10] Luu Y, Kim K, Hsiao B, Chu B, Hadjiargyrou M. Development of a nanostructured DNA delivery scaffold via electrospinning of PLGA and PLA–PEG block copolymers. J Control Release 2003;89:341–53.
[11] Kenawy ER, Bowlin GL, Mansfield K, Layman J, Simpson DG, Sanders EH, et al. Release of tetracycline hydrochloride from electrospun poly (ethylene-co-vinylacetate), poly (lactic acid), and a blend. J Control Release 2002;81:57–64.
[12] Jiang H, Hu Y, Li Y, Zhao P, Zhu K, Chen W. A facile technique to prepare biodegradable coaxial electrospun nanofibers for controlled release of bioactive agents. J Control Release 2005;108:237–43.
[13] Bölgen N, Vargel I, Korkusuz P, Menceloğlu YZ, Pişkin E. In vivo performance of antibiotic embedded electrospun PCL membranes for prevention of abdominal adhesions. J Biomed Mater Res Part B 2007;81:530–43.
[14] Xu X, Yang L, Wang X, Chen X, Liang Q, Zeng J, et al. Ultrafine medicated fibers electrospun from W/O emulsions. J Control Release 2005;108:33–42.
[15] Qi H, Hu P, Xu J, Wang A. Encapsulation of drug reservoirs in fibers by emulsion electrospinning: morphology characterization and preliminary release assessment. Biomacromolecules 2006;7:2327–30.
[16] Yoo HS, Kim TG, Park TG. Surface-functionalized electrospun nanofibers for tissue engineering and drug delivery. Adv Drug Deliv Rev 2009;61:1033–42.
[17] Shen X, Yu D, Zhu L, Branford-White C, White K, Chatterton NP. Electrospun diclofenac sodium loaded Eudragit® L 100-55 nanofibers for colon-targeted drug delivery. Int J Pharm 2011;408:200–7.
[18] Wang C, Yan KW, Lin YD, Hsieh PCH. Biodegradable core/shell fibers by coaxial electrospinning: processing, fiber characterization, and its application in sustained drug release. Macromolecules 2010;43:6389–97.
[19] Xu X, Chen X, Ma P, Wang X, Jing X. The release behavior of doxorubicin hydrochloride from medicated fibers prepared by emulsion-electrospinning. Eur J Pharm Biopharm 2008;70:165–70.
[20] Moghe AK, Gupta BS. Co-axial electrospinning for nanofiber structures: preparation and applications. Polym Rev 2008;48:353–77.
[21] Qi R, Cao X, Shen M, Guo R, Yu J, Shi X. Biocompatibility of electrospun halloysite nanotube-doped poly (lactic-co-glycolic acid) composite nanofibers. J Biomater Sci-Polym Ed 2012;1:299–313.
[22] Qi R, Shen M, Cao X, Guo R, Tian X, Yu J, et al. Exploring the dark side of MTT viability assay of cells cultured onto electrospun PLGA-based composite nanofibrous scaffolding materials. Analyst 2011;136:2897–903.
[23] Zhao Y, Wang S, Guo Q, Shen M, Shi X. Hemocompatibility of electrospun halloysite nanotube- and carbon nanotube-doped composite poly(lactic-co-glycolic acid) nanofibers. J Appl Polym Sci 2012. http://dx.doi.org/10.1002/APP.38054.
[24] Zhang J, Wang Q, Wang A. In situ generation of sodium alginate/hydroxyapatite nanocomposite beads as drug-controlled release matrices. Acta Biomater 2010;6:445–54.
[25] Mizushima Y, Ikoma T, Tanaka J, Hoshi K, Ishihara T, Ogawa Y, et al. Injectable porous hydroxyapatite microparticles as a new carrier for protein and lipophilic drugs. J Control Release 2006;110:260–5.
[26] Ma Z, Kotaki M, Yong T, He W, Ramakrishna S. Surface engineering of electrospun polyethylene terephthalate (PET) nanofibers towards development of a new material for blood vessel engineering. Biomaterials 2005;26:2527–36.
[27] Kim K, Luu YK, Chang C, Fang DF, Hsiao BS, Chu B, et al. Incorporation and controlled release of a hydrophilic antibiotic using poly(lactide-co-glycolide)-based electrospun nanofibrous scaffolds. J Control Release 2004;98:47–56.
[28] Lowy FD. *Staphylococcus aureus* infections. N Engl J Med 1998;339:520–32.
[29] Boyle VJ, Fancher ME, Ross Jr RW. Rapid, modified Kirby-Bauer susceptibility test with single, high-concentration antimicrobial disks. Antimicrob Agents Chemother 1973;3:418–24.
[30] Wang S, Wen S, Shen M, Guo R, Cao X, Wang J, et al. Aminopropyltriethoxysilane-mediated surface functionalization of hydroxyapatite nanoparticles: synthesis, characterization, and in vitro toxicity assay. Int J Nanomed 2011;6:3449–59.
[31] Guo YP, Yao YB, Guo YJ, Ning CQ. Hydrothermal fabrication of mesoporous carbonated hydroxyapatite microspheres for a drug delivery system. Microporous Mesoporous Mat 2012;155:245–51.
[32] Chandra VS, Baskar G, Suganthi RV, Elayaraja K, Joshy MIA, Venkatraman G, et al. Blood compatibility of iron doped nano hydroxyapatite and its drug release. ACS Appl Mater Interfaces 2012;4:1200–10.
[33] Kaur SP, Rao R, Nanda S. Amoxicillin: a broad spectrum antibiotic. Int J Pharm Pharm Sci 2011;3:30–7.
[34] Bebu A, Szabó L, Leopold N, Berindean C, David LIR. Raman, SERS and DFT study of amoxicillin. J Mol Struct 2011;993:52–6.
[35] Bisson-Boutelliez C, Fontanay S, Finance C, Kedzierewicz F. Preparation and physicochemical characterization of amoxicillin β-cyclodextrin complexes. AAPS PharmSciTech 2010;11:574–81.
[36] Suganthi RV, Elayaraja K, Joshy MI, Chandra VS, Girija EK, Kalkura SN. Fibrous growth of strontium substituted hydroxyapatite and its drug release. Mater Sci Eng 2011;31:593–9.
[37] Liu F, Guo R, Shen M, Cao X, Mo X, Wang S, et al. Effect of the porous microstructures of poly (lactic-co-glycolic acid)/carbon nanotube composites on the growth of fibroblast cells. Soft Mater 2010;8:239–53.
[38] Liu F, Guo R, Shen M, Wang S, Shi X. Effect of processing variables on the morphology of electrospun poly [(lactic acid)-co-(glycolic acid)] nanofibers. Macromol Mater Eng 2009;294:666–72.